Journal of Zhejiang University-SCIENCE A 2026 27(5):534-548
www.jzus.zju.edu.cn; www.springer.com/journal/11582
E-mail: jzus_a@zju.edu.cn

Research Article
https://doi.org/10.1631/jzus.A2500339

Check for updates

Effects of ultrasonic treatment on wet mineralization of cement powder

Yongsheng CHEN[1,2*], Fengping YU[3*], Yanbiao ZHU[4], Hedong LI[1,2✉], Tao WANG[5]

[1]*School of Civil Engineering and Architecture, Zhejiang Sci-Tech University, Hangzhou 310018, China*
[2]*Zhejiang Key Laboratory of Green, Digital, and Intelligent (GDI) Renovation for Urban Infrastructures, Hangzhou 310018, China*
[3]*Zhejiang Zheneng Technology & Environment Group Co., Ltd., Hangzhou 310012, China*
[4]*Lanxi Tianda Environmental Protection Building Materials Co., Ltd., Jinhua 321110, China*
[5]*State Key Laboratory of Clean Energy Utilization, Zhejiang University, Hangzhou 310027, China*

Abstract: In this study, an ultrasonic-assisted wet mineralization process is developed using ordinary Portland cement as the raw material. This approach is designed to advance the use of mineralization technologies in construction materials by simultaneously enhancing mechanical properties and mineralization efficiency. A comprehensive microstructural analysis is conducted to elucidate the underlying mineralization mechanisms facilitated by ultrasonic treatment. Furthermore, an industrial-scale implementation framework is developed to support the practical application of this technique. We find that the pH variation during the process follows three distinct stages: a rapid drop, a plateau, and a gradual decline. During the same wet mineralization period, the content of calcium silicate hydrate (C-S-H) in the ultrasonic-assisted cement suspension is increased by 16.02%. Ultrasonic-assisted treatment improves the degree of mineralization and suppresses the growth of large crystals. Moreover, the incorporation of wet mineralization-treated suspensions into cement pastes significantly increases the compressive strength of the cementitious system. The most notable enhancement is observed when ultrasonic-assisted wet mineralization is conducted for 15 min, which results in a 25.78% increase in 1-d compressive strength and a 12.20% improvement in 28-d compressive strength. A 25-min ultrasonic-assisted treatment gives the greatest reduction in setting time, shortening the initial setting time by 19.46% and the final setting time by 12.98%. Based on a calculated ultrasonic mineralization energy efficiency factor, we determine that the ultrasonic-assisted wet mineralization process achieves its highest efficiency within the first 5 min. Prolonged mineralization results in a noticeable decline in mineralization efficiency.

Key words: Wet mineralization; Ultrasonic action; Cement-based material; Cement suspension

1 Introduction

Cement serves as a fundamental building material that is used extensively in modern architecture and infrastructure development. However, its manufacturing process is associated with significant emissions. Statistical data indicate that cement production contributes to about 8% of global anthropogenic CO_2 emissions, exerting a considerable influence on global warming and environmental changes (Lippiatt et al., 2020; Li L and Wu, 2022). Therefore, reducing carbon emissions within the cement industry, or identifying feasible methods for capturing and storing the emitted CO_2, represents a critical strategy for addressing climate change.

Carbon capture and storage (CCS) technology, being a pivotal strategy for climate change mitigation, has attracted considerable attention and has been studied extensively across various disciplines in recent years. Cement-based materials, owing to their intrinsic alkalinity and the release of alkaline cations like Ca^{2+} during hydration, show a natural tendency toward CO_2 adsorption and mineralization (Gartner and Hirao, 2015; Ashraf, 2016; Shen et al., 2022a). Specifically, under optimal conditions of temperature, humidity, and carbon exposure, cementitious materials can undergo mineralization reactions with CO_2, forming stable compounds like calcium carbonate ($CaCO_3$), thereby achieving

✉ Hedong LI, lihedong@zstu.edu.cn
* The two authors contributed equally to this work
Hedong LI, https://orcid.org/0000-0002-0911-1976

Received July 24, 2025; Revision accepted Dec. 23, 2025;
Crosschecked Apr. 1, 2026; Online first May 6, 2026

long-term CO_2 sequestration. Monkman et al. (2016) conducted an experiment where a controlled amount of CO_2 was introduced during the concrete mixing phase. The results show that this method can significantly reduce both the initial and final setting time of concrete while enhancing early-age strength development. According to their findings, CO_2 reacts with the calcium components in cement particles to rapidly form micro-nano scale $CaCO_3$ particles. These particles, characterized by their high specific surface area and surface reactivity, act as nucleation centers that promote the attraction of hydration reactants, thereby accelerating the hydration process. However, the study also reveals that exceeding a certain threshold of injected CO_2 may lead to the formation of overly dense $CaCO_3$ coatings, which hinder further reactions and reduce overall effectiveness. In similar studies, He et al. (2017) directly introduced CO_2 during the cement mixing phase for mineralization treatment. Although this method effectively increases CO_2 absorption in the cement system, it also leads to a decline in certain mechanical properties, particularly evident in the slower development of later-stage strength. Wang ML et al. (2023) extended the stirring time during the carbonization process and found that the mechanical properties were improved. However, compared with cement paste that has not undergone mineralization treatment, there is still some reduction in performance.

Ultrasonic dispersion, as an external-field-assisted strengthening technology, offers a novel approach to overcome the above limitations. The ultrasonic cavitation effect has significant advantages in material synthesis and reactive mass transfer enhancement due to its unique mechano-chemical synergistic effects (Dong et al., 2016; Hamidi et al., 2017; Sulistiyono et al., 2019; Tamidi et al., 2021). Hamidi et al. (2017) confirmed through experiments on a gas–liquid system that an ultrasonic field can significantly increase the solubility of CO_2 in the liquid phase. This is attributed to the cavitation effect, which improves some properties of the liquid phase. Sulistiyono et al. (2019) introduced ultrasonic dispersion technology in the synthesis process of $CaCO_3$, effectively inhibiting the phenomenon of particle agglomeration and successfully preparing nano-scale calcium carbonate with an average particle size of 64 nm. Xu et al. (2023) used an ultrasonic dispersion-assisted stirring process during the mixing of cement paste. Their results show that the hydration rate of cement particles is significantly increased. The cavitation effect peels off the hydration products on the surface of cement particles, and at the same time, the micro-turbulence caused by the collapse of cavitation bubbles enhances the frequency of particle collisions. Xiong et al. (2024) confirmed that ultrasonic treatment reduced the porosity of cement paste and found that the period of induction of cement hydration was shortened. Liu LL et al. (2021) innovatively introduced ultrasonic dispersion during the mixing of fresh cement paste coupled with CO_2 injection. The process enhances both the rate of uptake of CO_2 and the compressive strength of the paste, but overall mineralization efficiency remains limited due to the constraints of the mixing stage. Moreover, their study focuses mainly on workability, lacking a comprehensive phase analysis of how ultrasonic treatment influences the mineralization mechanism.

Wet mineralization technology serves as an effective approach for CO_2 storage. This technology involves mainly placing solid building materials containing alkaline components in a liquid-phase environment, introducing CO_2 gas under high water-to-binder ratio conditions, and promoting reactions with alkaline cations such as Ca^{2+} and Mg^{2+} to form carbonate precipitates, thereby achieving long-term CO_2 sequestration (Lippiatt et al., 2020; Zajac et al., 2020; Shen et al., 2022b; Li WZ et al., 2023; Mao et al., 2023; Fu et al., 2024). Under wet conditions, the solubility of CO_2 in water increases, leading to the formation of carbonic acid or bicarbonate ions. Moreover, the presence of water enhances the dispersion of solid particles and ion diffusion (Mao et al., 2023), significantly improving contact efficiency at the reaction interface and accelerating the mineralization reaction rate (Fagerlund et al., 2012; Liu SH et al., 2021b). However, the current mainstream wet mineralization method relies on mechanical stirring. Mechanical stirring, due to its limited dispersing ability, is unable to overcome the interfacial binding energy of the mineralized product layer (C-S-H/$CaCO_3$ complex), resulting in continuous thickening of the product layer. Here, C-S-H is calcium silicate hydrate. This restricts the diffusion ability of Ca^{2+} and the progress of the mineralization reaction. By integrating ultrasonic dispersion technology with wet mineralization and using the energy concentration and localized strong disturbance effects of ultrasonic cavitation, we expect that the compactness of the product layer can be further

reduced, the "passivation" effect of the $CaCO_3$ coating on the reaction process can be mitigated, and the conversion efficiency and uniformity of the mineralization reaction can be enhanced.

Based on established mineralization techniques, in this study, we develop an ultrasonic-assisted wet mineralization process. Conventional methods relying solely on mechanical stirring generally yield limited mineralization efficiency. While previous attempts have introduced ultrasonic dispersion during the mixing of low water-to-binder ratio pastes, the high viscosity of the system and the constrained reaction time restrict the degree of mineralization, making deep treatment difficult to achieve. By integrating ultrasonic dispersion technology into a wet mineralization system, our proposed approach significantly enhances mineralization efficiency while simultaneously improving the comprehensive performance of the cement-based materials. In the experimental design, a fresh cement-water system is established, and CO_2 gas is introduced while maintaining a high water-to-binder ratio. An ultrasonic field is simultaneously applied during this process. Microstructural characterization techniques, including X-ray diffraction (XRD), Fourier transform infrared spectroscopy (FT-IR), scanning electron microscopy (SEM), and thermogravimetric analysis (TGA), are used to thoroughly examine the influence of ultrasound-assisted technology on the morphology, phase composition, and reaction pathways of the mineralized products. Furthermore, to assess its practical application potential, the cement suspension treated by ultrasound-assisted wet mineralization is incorporated into a conventional cement paste system. The early strength development, setting time, and 28-d compressive strength are evaluated, and the strengthening mechanism of this technology on cement performance is analyzed. Finally, we evaluate the energy efficiency of the ultrasonic-assisted wet mineralization process and develop a scalable framework for its industrial implementation.

2 Material and experiments

The cement used in this study is ordinary Portland cement (P.O. 52.5). The oxide composition of the cement is obtained through X-ray fluorescence (XRF) analysis (Table 1). Table 2 shows the names of the samples and the experimental conditions of each sample. The water used for the experiment is municipal tap water. The carbon dioxide is supplied by the Hangzhou Zhejiang Gas Co., Ltd., China, with a purity of 99.0%. The water-cement ratio of the cement suspension is 5:1. We elucidate the mechanism of ultrasonic-assisted wet mineralized cement suspension using pH measurement, XRD, FT-IR, TGA, and SEM, while assessing macroscopic performance through compressive strength and setting time. The macroscopic test specimen is cement paste. The wet mineralization of cement substitution rate is 8%, and the water-cement ratio of the cement paste specimen is 0.4. Detailed experimental specifications can be found in Section S1 of the electronic supplementary materials (ESM). The experimental flow chart is shown in Fig. S1 of the ESM.

3 Results and discussion

3.1 Analysis of temperature changes

Fig. 1 illustrates the temperature evolution during the 25-min mineralization process for both the

Table 1 Composition of cement oxides

Oxide	Mass fraction (%)
Na_2O	0.471
SO_3	3.895
MgO	1.396
K_2O	0.751
Al_2O_3	5.353
SiO_2	21.988
CaO	61.260

Table 2 Samples tested under different conditions

Sample name	Treatment	CO_2 flow rate (L/min)	Mineralized cement substitution rate (%)	Mineralization duration (min)	Total CO_2 input volume (L)
UC-2-5	Ultrasonic	2	8	5	10
UC-2-15	Ultrasonic	2	8	15	30
UC-2-25	Ultrasonic	2	8	25	50
MC-2-25	Non-ultrasonic	2	8	25	50

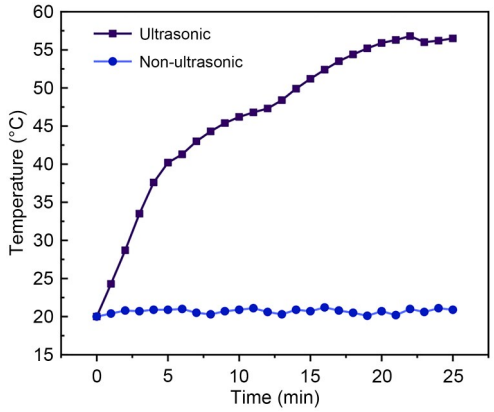

Fig. 1 Comparison of temperature changes of cement powder during ultrasonic-assisted and non-ultrasonic-assisted wet mineralization

ultrasonic-assisted and non-ultrasonic-assisted wet mineralization groups. Although both groups start at the same temperature of 20 °C, their thermal behavior exhibits significant differences.

The ultrasonic-assisted group shows substantial temperature variations, following a characteristic nonlinear heating trend, with the temperature rising from an initial 20.0 to 56.8 °C. This phenomenon is attributed mainly to the thermal effects induced by ultrasonic propagation in the medium (Xiong et al., 2023): Ultrasonic cavitation imparts significant kinetic energy to both fluid molecules and cement particles, converting acoustic energy into thermal energy through continuous mechanical vibration, expansion, and friction, thereby leading to a pronounced temperature increase in the system. From a kinetic perspective, the temperature change in the ultrasonic group shows distinct stages—the most notable increase occurs within the first 5 min, where the temperature rises rapidly from 20 °C to about 40 °C. Subsequently, the rate of heating gradually decelerates, eventually stabilizing around 56 °C.

In contrast, the non-ultrasonic group exhibits a relatively mild temperature change, remaining within a narrow range of 20–21 °C. Although both mineralization and hydration reactions of cement are exothermic in nature, the high water-to-binder ratio of the suspension effectively absorbs the reaction heat. Combined with the absence of ultrasonic energy input, this results in a negligible overall temperature increase in the system.

3.2 Analysis of pH changes

A comparison of pH changes between ultrasonic and non-ultrasonic-assisted wet mineralization of cement is shown in Fig. 2. The pH variation can be categorized into three distinct stages: a rapid drop, a subsequent plateau, and a final gradual decline. A detailed diagram of the mechanism of pH variation can be found in Fig. S2 of the ESM.

3.2.1 Rapid drop

Initially, the pH of the cement suspension is 11.7, which results from the dissolution and hydration of cement powder. Upon the onset of carbonation, the pH rapidly decreases from 11.7 to about 8.0, mainly due to the rapid consumption of calcium hydroxide ($Ca(OH)_2$, CH) (Chang et al., 2018; Mehdipour et al., 2019; Wang and Chang, 2019; Goergens et al., 2020; Aghajanian et al., 2021), a product of cement hydration. During the premixing stage, cement mineral components such as tricalcium silicate (C_3S) and dicalcium silicate (C_2S) undergo hydration reactions upon contact with

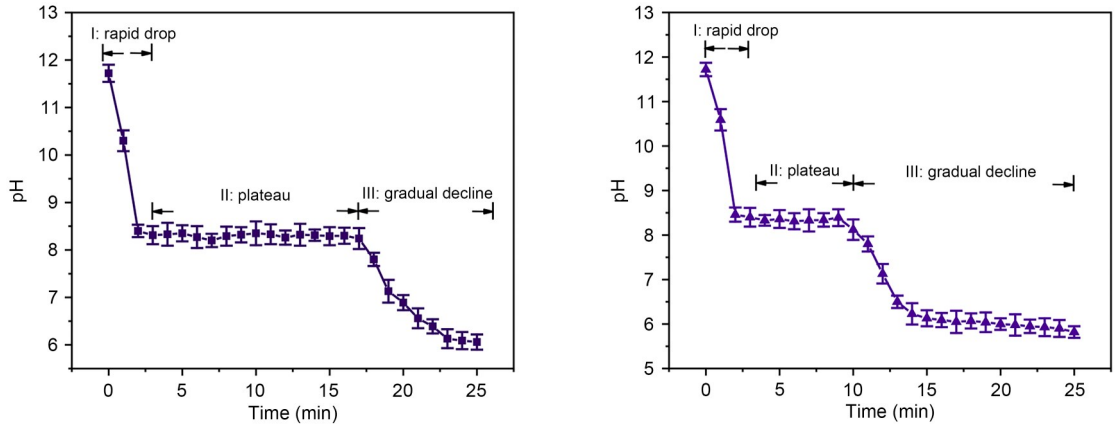

Fig. 2 Comparison of pH changes of cement powder by different wet mineralization: (a) ultrasonic-assisted; (b) non-ultrasonic-assisted

water, producing CH and C-S-H gel, as shown in chemical Eqs. (1) and (2). CH, being the main alkaline compound, contributes to the high pH environment. When CO_2 is introduced, it dissolves in the liquid phase to form carbonic acid (H_2CO_3). Subsequently, CH reacts with H_2CO_3 to precipitate $CaCO_3$, consuming OH^- ions in the process. This reaction leads to a significant drop in the pH. The reaction rate during this stage is influenced by the mass transfer efficiency of CO_2 dissolution and the dissolution kinetics of CH.

$$3CaO\cdot SiO_2+(n+3-x)H_2O\rightarrow xCaO\cdot SiO_2\cdot nH_2O+(3-x)Ca(OH)_2, \quad (1)$$

$$2CaO\cdot SiO_2+(n+2-x)H_2O\rightarrow xCaO\cdot SiO_2\cdot nH_2O+(2-x)Ca(OH)_2. \quad (2)$$

3.2.2 Plateau

After the pH value drops to 8.0–8.5, the pH plateaus, indicating that the CH is formed when the premixing has been completely consumed. During this pH plateau stage, three major reaction pathways contribute to mineralization: (1) CH is produced from the ongoing hydration of C_3S and C_2S continues to react with CO_2, consistent with the reactions occurring in the rapid drop; (2) C_3S directly participates in mineralization by reacting with CO_2; (3) C_2S similarly undergoes direct mineralization with CO_2. The mineralization of CH takes precedence over that of C_3S and C_2S, meaning that CH is preferentially consumed (Shen et al., 2022a). The continuous hydration of C_3S and C_2S, coupled with the concurrent mineralization of CH, C_3S, and C_2S, establishes a dynamic equilibrium. This balance continuously consumes H^+ and OH^- ions in the suspension, thereby stabilizing the pH value. From a macroscopic perspective, this corresponds to a dynamic equilibrium between the leaching rate of Ca^{2+} and the dissolution rate of CO_2. The released Ca^{2+} follows two main pathways: One portion undergoes hydration followed by mineralization, while the other participates directly in the mineralization reaction. Despite the reduction in CO_2 solubility caused by ultrasonic heating, the process simultaneously enhances the leaching kinetics of Ca^{2+}. This accelerated release of calcium ions shifts the reaction equilibrium forward, thereby increasing the CO_2 dissolution rate and overall reaction kinetics. Thus, the reaction rate is higher in the ultrasonic group than that in the non-ultrasonic group at this stage. The reaction process is kinetically constrained by the dissolution rates of the mineral phases and the formation rate of the product layer (He et al., 2017). The plateau for the ultrasonic-assisted group lasts until about 17 min, compared with only 9 min in the non-ultrasonic group (Fig. 2). Thus, ultrasonic treatment significantly extends the plateau. This phenomenon can be attributed to the surface of cement particles in the non-ultrasonic group becoming coated with a dense composite layer of C-S-H gel and $CaCO_3$ during the early plateau, forming an ion barrier that inhibits further Ca^{2+} release. In contrast, the ultrasonic-assisted wet mineralization system achieves sustained Ca^{2+} leaching rates through a dual mechanism of ultrasonic cavitation. The thermal effect enhances ion migration and diffusion kinetics, while the mechanical stresses generated by cavitation-induced microjets and shock waves dynamically suppress the formation of a dense product composite layer, thereby continuously exposing fresh reaction surfaces and maintaining calcium ion dissolution.

3.2.3 Gradual decline

At this stage, the surface of cement particles is coated with a significantly thicker reaction product layer, consisting of a C-S-H/$CaCO_3$ composite. The $CaCO_3$ and C-S-H gel form an intricately intertwined structure, which hinders ion diffusion and acts as an effective ion diffusion barrier. This densification of the product layer leads to a marked reduction in the leaching rate of Ca^{2+}, making its leaching efficiency lower than that of CO_2. Despite the constant rate of carbon passage, the accumulation rate of H^+ slows down during this stage. As shown in Fig. 2, the final pH values for both groups approach that of carbonic acid, indicating near saturation of CO_2 solubility in the suspension and near the limit of CO_2 absorption. The pH value shows a gradual downward trend. Notably, the onset of the slow descent period occurs earlier in the non-ultrasonic group than that in the ultrasonic group, suggesting that regulation of the product layer structure prolongs the effective duration of the reaction.

3.3 XRD analysis

The results of XRD analysis of the cement powder suspensions used in wet mineralization, both with and without ultrasonic treatment, are presented in Fig. 3. The main phases identified in the cement powder during wet mineralization include calcite, C_3S, and C_2S. The

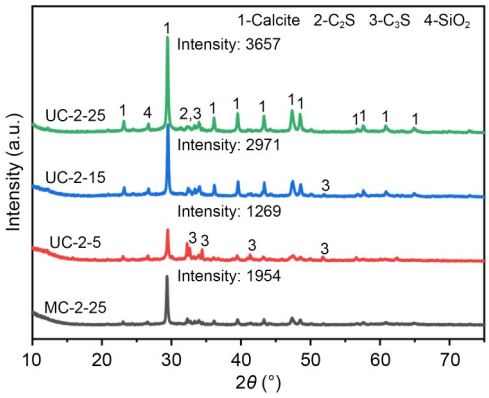

Fig. 3 XRD spectra of ultrasonic-assisted and non-ultrasonic-assisted wet mineralization of cement suspensions

data indicate that both C_3S and C_2S persist in all samples, suggesting that the cement powder has not undergone complete mineralization. Moreover, the absence of CH in the XRD spectra confirms its full reaction, which is consistent with the results from the previous pH test. Note that calcite is the only crystalline form of calcium carbonate observed. This phenomenon can be attributed to the high water-to-binder ratio of suspension, which provides a favorable environment for sufficient contact and reaction between calcium ions and carbonate ions. As a result, the mineralization process proceeds efficiently, allowing the metastable polymorphs such as vaterite and aragonite to transform completely into the thermodynamically most stable form—calcite.

Fig. 3 shows that in the ultrasonic-assisted group (ultrasonic-assisted carbonization (UC) series), the calcite content of wet mineralization exhibits a nonlinear increase trend with the extension of mineralization time. Notably, the increase of calcite during the initial 15 min of mineralization (UC-2-5 to UC-2-15) is significantly higher than the growth rate over the subsequent 10 min (UC-2-15 to UC-2-25). This attenuation in the rate of calcite formation is closely associated with the development of composite layers of reaction products: Rapid consumption of CH dominates the initial mineralization phase when the cement particle surface has not yet formed a dense product layer and the Ca^{2+} leaching rate is high. As the reaction progresses, C-S-H gel deposits along with $CaCO_3$ to form a coating that inhibits further dissolution of internal minerals, leading to a decrease in the reaction rate. The calcite peak intensity of UC-2-15 is comparable to that of UC-2-25, indicating similar extents of mineralization reaction between UC-2-15 and UC-2-25. UC-2-15 essentially represents the plateau stage depicted in Fig. 2. Effectively prolonging this homeostasis period will enhance the efficiency of wet mineralization. Both UC-2-15 and UC-2-25 exhibit significantly higher calcite content than MC-2-25. Given the established positive correlation between calcite content and mineralization duration, it can be reasonably deduced that the 15-min mechanically stirred system will produce a lower calcite content than that of MC-2-25. Consequently, these results confirm that under equivalent processing time (15 min), the calcite content of the 15-min ultrasonic-assisted system (UC-2-15) will exceed that of its mechanically stirred counterpart, demonstrating that ultrasonic treatment effectively enhances the overall mineralization efficiency in wet mineralization systems.

3.4 FT-IR analysis

The FT-IR spectra of ultrasonic-assisted and non-ultrasonic-assisted wet mineralization of cement paste suspensions are presented in Fig. 4. FT-IR spectroscopy can detect structural changes in mineralized and hydrated products, as well as other phases. According to previous studies (Shen et al., 2022a), the absorption bands around 1400, 870, and 710 cm^{-1} correspond to C–O bond vibrations, while those around 900 and 1100 cm^{-1} are associated with Si–O bond vibrations (Fernández-Carrasco et al., 2012; Liu SH et al., 2021a). The absorption band at about 1400 cm^{-1} represents stable C–O bonds indicative of well-crystallized $CaCO_3$, whereas those around 870 and 710 cm^{-1} represent less stable C–O bonds characteristic of amorphous calcium carbonate (Günther et al., 2005; Zou et al., 2015). As the ultrasonic-assisted wet mineralization time increases, the intensity of the absorption signal at 1400 cm^{-1} gradually strengthens, indicating an increase in the amount of well-crystallized calcium carbonate. Additionally, at the same carbonation time, the C–O bond absorption peak for UC-2-25 shifts to a higher wavenumber (1442 cm^{-1}) than that of MC-2-25 (1417 cm^{-1}), suggesting a higher degree of C–O bond polymerization and a more stable crystalline structure.

FT-IR can be used for the quantitative analysis of C-S-H content and proportion during the wet mineralization process. Two overlapping absorption bands are observed within the Si–O bond region (Fig. 4). The broad band near 1000 cm^{-1} corresponds to the

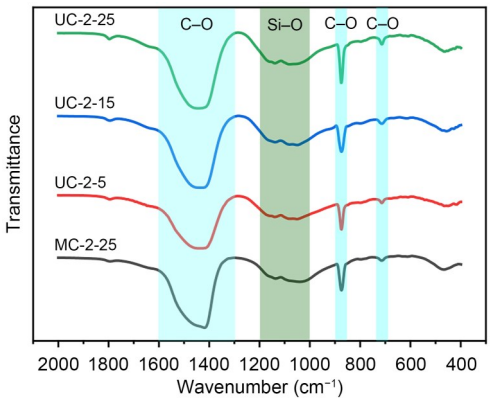

Fig. 4 FT-IR spectra of ultrasonic-assisted and non-ultrasonic-assisted wet mineralization of cement suspensions

asymmetric tensile vibration of the Si–O bond in the initial high-calcium C-S-H. CO_2 reacts with the interlayer and defect-associated calcium in the C-S-H chain structure, forming $CaCO_3$ and leading to the detachment of calcium from the chains (Mao et al., 2023). The decalcified C-S-H exhibits a high degree of polymerization (Shen et al., 2022a). The wide band near 1100 cm^{-1} is attributed to the decalcification of the initial high-calcium C-S-H after mineralization, leading to low-calcium C-S-H with a higher degree of polymerization.

Previous studies have demonstrated the feasibility of decoupling FT-IR spectra for the quantitative analysis of amorphous phases such as C-S-H (Sáez del Bosque et al., 2014; Mao et al., 2023). In this study, Gaussian fitting is applied to the FT-IR spectra in the 900–1200 cm^{-1} region, the range corresponding to the Si–O bond, revealing a strong correlation (Fig. 5). The deconvolution process separates the original overlapping peaks into two distinct peaks, with the peak areas representing the relative contents of high-calcium and low-calcium C-S-H, respectively (Table 3). Additionally, the total peak area of C-S-H, which is the sum of the peak areas of high-calcium and low-calcium C-S-H, increases with prolonged ultrasonic wet mineralization time, indicating an increase in C-S-H

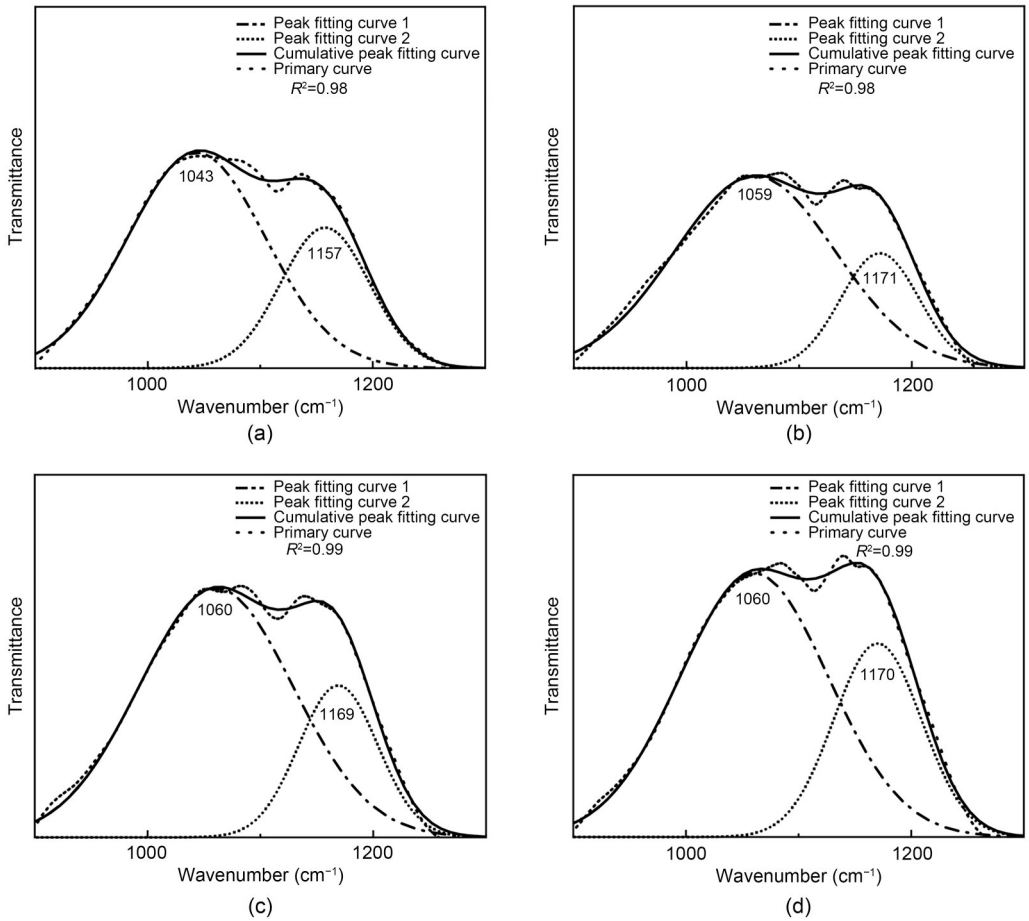

Fig. 5 FT-IR spectra split-peak fitting results in the 900 to 1200 cm^{-1} band: (a) MC-2-25; (b) UC-2-5; (c) UC-2-15; (d) UC-2-25

Table 3 Content and proportions of high-calcium C-S-H and low-calcium C-S-H in the wet mineralization process of cement powder suspensions under variable conditions

Sample name	Peak area of high-calcium C-S-H gel	Peak area of low-calcium C-S-H gel	Total area of C-S-H peaks	High-calcium C-S-H gel content (%)	Low-calcium C-S-H gel content (%)
MC-2-25	2850.86	1355.28	4206.14	67.78	32.22
UC-2-5	2728.26	928.13	3656.39	74.62	25.38
UC-2-15	3310.65	1246.56	4557.21	72.65	27.35
UC-2-25	3414.03	1465.74	4879.77	69.96	30.04

content. Consequently, during the wet mineralization process, both mineralization and hydration reactions occur concurrently, leading to a coupled reaction between mineralization and hydration.

The total C-S-H peak areas for UC-2-5, UC-2-15, and UC-2-25 are 3656.39, 4557.21, and 4879.77, respectively, while that of MC-2-25 is 4206.14 (Table 3). The growth rate of C-S-H during the initial 5 to 15 min for ultrasonic-assisted wet mineralization is 90.08 min^{-1}, which subsequently decreases to 32.26 min^{-1} between 15 and 25 min, indicating the onset of an equilibrium stage. This suggests that the reaction rate remains highly efficient even during the plateau stage. Furthermore, under identical reaction conditions, the total peak areas of both UC-2-25 and UC-2-15 surpass that of MC-2-25, indicating a higher C-S-H gel content in their cement suspensions. The total peak area of C-S-H in UC-2-25 is 16.02% higher than that in MC-2-25. Therefore, it can be inferred that ultrasonic action increases the C-S-H content by 16.02%. This leads to the reasonable inference that the C-S-H content of UC-2-15 will also exceed that of the mechanically stirred system with a shorter reaction time of 15 min. This phenomenon is attributed to the ultrasonic cavitation and thermal effects, which significantly accelerate the hydration process of cement particles.

The proportion of low-calcium C-S-H in Table 3 serves as an indirect indicator of the extent of C-S-H decalcification. Sample MC-2-25 shows the highest degree of decalcification, with a low-calcium C-S-H content of 32.22%, which is slightly higher than that of UC-2-25 at 30.04%. This difference can likely be attributed to the different pH levels of the suspensions (Shen et al., 2022a). Prior research indicates that the polymerization of C-S-H gel occurs more effectively under acidic conditions. The pH of MC-2-25 is marginally lower than that of UC-2-25 (Fig. 2), thereby promoting the transformation of high-calcium C-S-H into the more polymerized low-calcium C-S-H (Shen et al., 2022a).

3.5 Thermogravimetric analysis

The thermogravimetric (TG) and derivative thermogravimetric (DTG) results for the ultrasonic-assisted and non-ultrasonic-assisted wet mineralization of cement suspensions are presented in Fig. 6. The troughs are predominantly concentrated near 700 °C, corresponding to well-crystallized calcium carbonate. This indicates that the calcium carbonate formed in the cement suspension exhibits relatively high crystallinity. Additionally, the troughs in Fig. 6 progressively shift to higher temperatures, suggesting an increase in the thermal stability of the mineralized product, $CaCO_3$. Notably, the stability of $CaCO_3$ in MC-2-25 is only marginally higher than that in UC-2-5.

By quantitatively comparing the actual CO_2 absorption of the cement suspension to its maximum potential CO_2 absorption, the degree of mineralization (α) of the cement suspension can be determined (Eq. (3)). $\eta_{\mathrm{exp}CO_2}$ in Eq. (3) denotes the actual sequestrated CO_2 of the cement suspension and $\eta_{\mathrm{theo}CO_2}$ denotes the theoretical sequestrated CO_2. The actual sequestrated CO_2 can be estimated based on the percentage of mass loss occurring near 700 °C during TGA. The methodology for calculating the theoretical sequestrated CO_2 of a cement suspension is provided in Eq. (4) (Steinour, 1959; Andrade and Sanjuán, 2021).

$$\alpha = \frac{\eta_{\mathrm{exp}CO_2}}{\eta_{\mathrm{theo}CO_2}} \times 100\%, \tag{3}$$

$$\eta_{\mathrm{theo}CO_2} = \frac{M_{CO_2}}{M_{CaO}}[\mu_{CaO} - 0.7\mu_{SO_2}] + 1.09\mu_{MgO} + 0.71\mu_{Na_2O} + 0.4675\mu_{K_2O}. \tag{4}$$

Here, M_{CO_2} and M_{CaO} denote the molar masses of CO_2 and CaO, respectively. μ_x in Eq. (4) denotes the

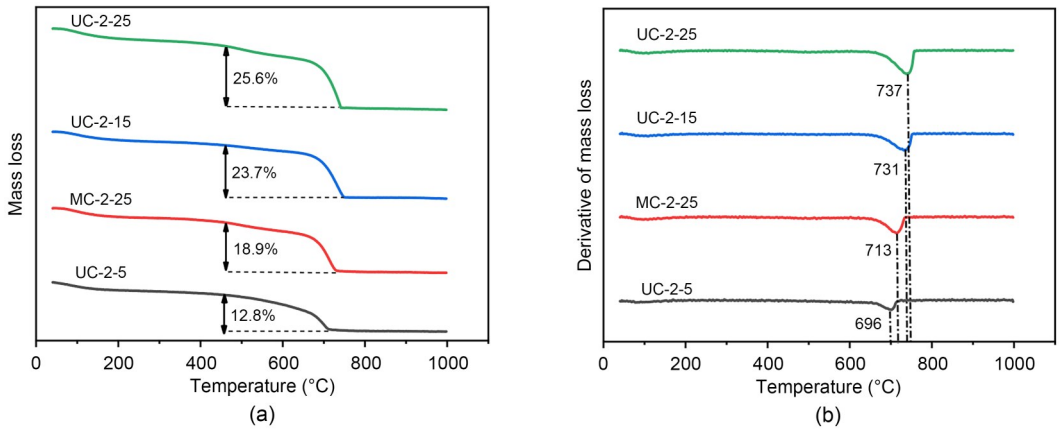

Fig. 6 TG and DTG results of ultrasonic-assisted and non-ultrasonic-assisted wet mineralization of cement suspensions: (a) TG; (b) DTG

mass fractions of CaO, SO_2, MgO, Na_2O, and K_2O, with specific values provided in Table 1. Based on calculation, the theoretical CO_2 sequestration capacity of this cement is 48.19 g/100 g of cement. The actual CO_2 sequestration amount for each suspension is then determined from the mass loss rate in the TG curves (Fig. 6a), and the results are summarized in Table 4.

Table 4 Comparison of mass loss rate, decomposition temperature, and degree of mineralization

Sample name	Mass loss rate (%)	Decomposition temperature (°C)	Degree of mineralization (%)
MC-2-25	18.9	713	39.34
UC-2-5	12.8	696	26.56
UC-2-15	23.7	731	49.18
UC-2-25	25.6	737	53.12

The degree of mineralization during ultrasonic-assisted wet mineralization progressively increases with the extension of carbon transfer time. Specifically, the mineralization degree for UC-2-5 is 26.56% after 5 min of ultrasonic-assisted wet mineralization and increases to 49.18% after 15 min, representing an increase of 22.62 percentage points (PPs). However, when the ultrasonic-assisted wet mineralization time is extended to 25 min, the mineralization degree reaches 53.12%, which is only 3.94 PPs higher than that observed at 15 min. These results indicate a positive correlation between the degree of mineralization and its duration. However, as mineralization proceeds, the thickening of the resulting composite product layer gradually reduces the mineralization efficiency. Under identical mineralization conditions, UC-2-15 exhibits a 9.84 PPs higher degree of mineralization than MC-2-25. Based on the established positive correlation between the degree of mineralization and carbonation duration, it can be inferred that the 15-min mechanically stirred system will show a lower degree of mineralization than that of MC-2-25 and thus will be significantly lower than that of UC-2-15. Therefore, although the elevated system temperature reduces CO_2 solubility in the suspension, the cavitation-induced erosion of the product layer enhances ion diffusion efficiency, while the associated thermal effect accelerates the reaction kinetics. Collectively, these synergistic effects lead to a significant improvement in the overall degree of mineralization in the ultrasonic-assisted group.

3.6 SEM analysis

SEM is used to characterize the mineralized products from the ultrasonic-assisted group (UC series) and mechanical mixing group (Fig. 7). This analysis elucidates the polymorphic characteristics of calcium carbonate crystals and the evolution patterns of the product layer under different process conditions. Samples exhibit regular small cube-like calcite ($CaCO_3$) crystals with nearly 90° angles, consistent with typical calcite growth characteristics. Comparative SEM image analysis reveals that while all samples exhibit product layer agglomeration, significant differences are observed in morphology and dispersion. A continuous covering layer is formed between the grains of UC-2-5 through C-S-H gel bridging (Fig. 7a), whereas continuous calcite grain accumulation is noted in UC-2-15, UC-2-25, and MC-2-25 (Figs. 7b–7d). This phenomenon can be attributed to the shorter carbonation passage

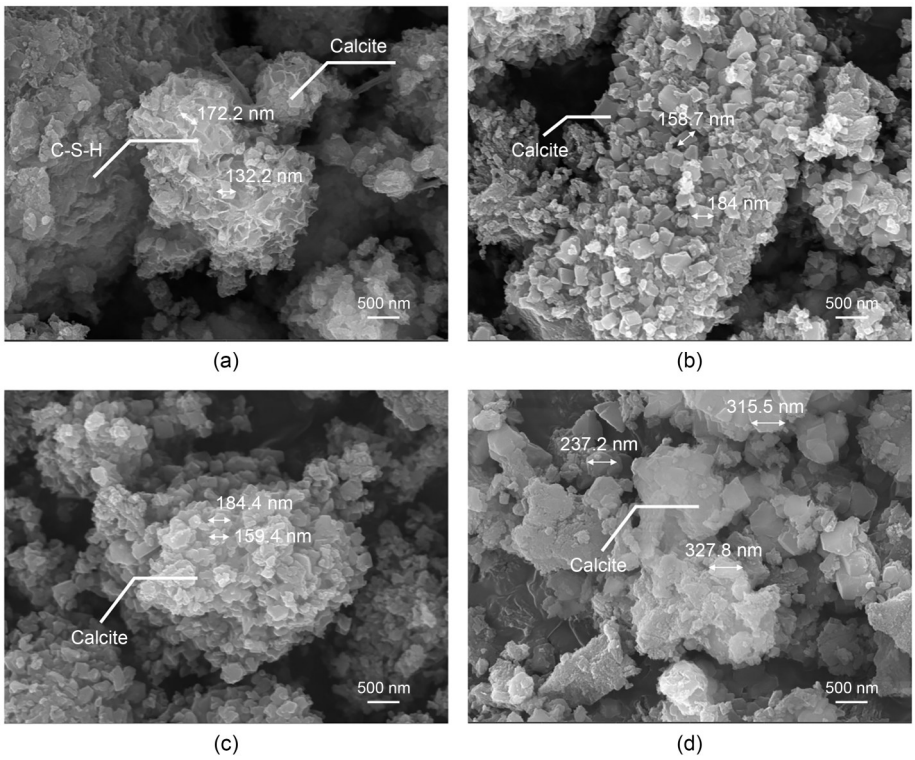

Fig. 7 SEM images of ultrasonic-assisted wet mineralization and non-ultrasonic-assisted wet mineralization of cement suspensions: (a) UC-2-5; (b) UC-2-15; (c) UC-2-25; (d) MC-2-25

time of UC-2-5, where pre-stirred C-S-H does not participate in mineralization or decalcification decomposition, resulting in reduced calcium carbonate production. Additionally, the size of calcite crystals in the ultrasonic-assisted group (UC-2-15 and UC-2-25) decreases significantly, with ultrasonic treatment inhibiting the growth of larger crystals. Scale comparison based on SEM images reveals that the grain sizes in the ultrasonic-assisted wet mineralization group (Figs. 7a–7c) range from 100 to 200 nm, while those in the conventional wet mineralization group (without ultrasonic treatment) fall within the 230–500 nm range.

3.7 Setting time

The setting time for different samples is presented in Fig. 8. Comparisons of setting time, standard deviation, and the rate of change relative to the control are presented in Table S1 of the ESM. Compared to the untreated control group (N, without adding ultrasonic-assisted wet mineralization cement suspension to the cement paste), the initial setting time of all experimental groups is reduced by 6.49% to 19.46%, while the final setting time is decreased by 5.90% to 12.98%.

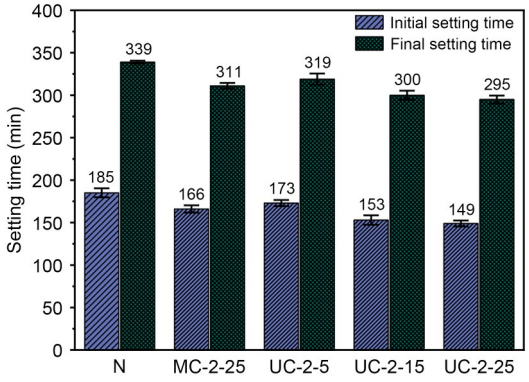

Fig. 8 Comparison of setting times

These results indicate that wet mineralization of the cement suspension effectively shortens the setting time of the cement paste. Under the same wet mineralization duration, the reduction effect of UC-2-25 on the initial setting time, relative to the control group N, is 9.19 PPs higher than that of MC-2-25. This improved performance can be attributed to the ultrasonic treatment generating finer crystals that provide dual benefits: a filling effect and early-stage hydration nucleation. It can be reasonably inferred that UC-2-15 would similarly exhibit higher early-age strength than its 15-min

mechanically stirred counterpart. Furthermore, comparisons among the last three groups (UC-2-5, UC-2-15, and UC-2-25) reveal the impact of variable ultrasonic-assisted wet mineralization time on setting time reduction. The effect of setting time reduction relative to carbon transfer time shows a nonlinear trend. Compared with UC-2-15, the reduction effects of UC-2-5 on the initial setting time and final setting time relative to the control group N are 10.80 PPs and 5.60 PPs lower, respectively. Compared with UC-2-15, the initial setting time of UC-2-25 is shortened by only 2.17 PPs, and the final setting time by 1.48 PPs. Evidently, when the duration of wet mineralization exceeds a certain critical threshold, the marginal benefit of reducing setting time diminishes significantly.

3.8 Compressive strength

The compressive strength for cement pastes partially substituted with cement suspensions at various ages are presented in Fig. 9. Comparisons of the percentage strength gain relative to the control (N, without adding ultrasonic-assisted wet mineralization cement suspension to the cement paste) are presented in Fig. S3 of the ESM. The overall trend in compressive strength is clear and statistically significant. Regardless of mineralization, the compressive strength of specimens shows a nonlinear increase with curing time. The strength of the experimental group after mineralization is consistently higher than that of the control group without mineralization. Across all ages, UC-2-15 demonstrates the highest compressive strength, followed by UC-2-25, while UC-2-5 exhibits the lowest strength. This may be attributed to insufficient reaction time for UC-2-5, leading to inadequate formation of $CaCO_3$ and C-S-H. Despite a longer reaction duration, group UC-2-25 exhibits the formation of a dense C-S-H/$CaCO_3$ composite layer on the cement particle surfaces. Although ultrasonic treatment partially disrupts this layer, its thickness and compactness continue to increase as the reaction proceeds, ultimately hindering further hydration of the unreacted inner particles. This observation aligns with the findings of Monkman et al. (2016), which indicates that an excessively thick product layer can significantly reduce ion permeability, thereby suppressing later-stage hydration and resulting in diminished gains in mechanical properties. In the present system, even with the introduction of ultrasonic agitation to delay densification, a critical threshold exists. Beyond 15 min, the continued growth of the product layer causes the reaction mechanism to shift from surface reaction control to diffusion control. Consequently, the marginal benefits in both the degree of mineralization and specimen strength development begin to decline. These results confirm that the mineralization process has a well-defined optimum duration, beyond which further extension does not enhance performance.

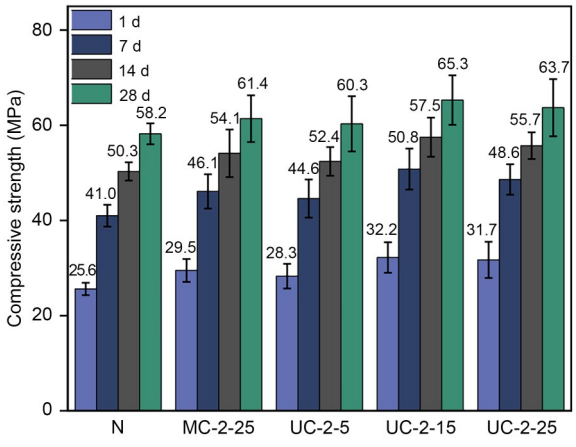

Fig. 9 Compressive strength of specimens at different ages

The compressive strengths of both UC-2-15 and UC-2-25 significantly exceed that of MC-2-25, suggesting that the inhibitory effect of the product composite layer on mechanical properties requires a critical mineralization threshold to be reached. Given that the degree of mineralization of MC-2-25 remains below this critical value, it can be reasonably deduced that the 15-min mechanically stirred system with a lower degree of mineralization will not provide greater strength enhancement to the cementitious matrix than that of MC-2-25. Consequently, the cement paste formed by using UC-2-15 as a partial cement substitute has a higher compressive strength than the suspension liquid that is mechanically stirred for 15 min. Compared to the untreated control group (N), the optimal performing formulation UC-2-15 shows a 25.78% increase in compressive strength at 1-d curing age, maintaining a significant 12.20% improvement after 28 d of curing. In contrast, the mechanically stirred mineralization group MC-2-25 shows corresponding gains of only 15.23% and 5.50%, respectively, with its strengthening effect merely exceeding that of UC-2-5, which undergoes a shorter ultrasonic treatment among the ultrasonic-assisted groups. These results confirm that UC-2-15 provides remarkable strength enhancement to the cement

paste within a relatively short mineralization period. With increasing curing age, the gain in strength of the four experimental groups gradually decreases, proving that the cement suspension after wet mineralization has certain early strength characteristics. It can accelerate the hydration of cement, but the gain in strength is more limited in specimens with a 28-d curing age.

3.9 Mechanism of ultrasonic-assisted wet mineralization

3.9.1 Mechanism of ultrasonic enhancement of mineralization efficiency

Ultrasonic waves are mechanical waves with frequencies exceeding 20 kHz, characterized by high frequency, short wavelength, and strong directivity. When ultrasonic waves propagate through a liquid medium, the periodic variation in sound pressure induces alternating compression and expansion of the medium's molecules. These cavitation nuclei undergo a three-stage dynamic evolution of expansion, contraction, and collapse under the energy-driven effect of the acoustic field. During the rarefaction half-cycle, when the sound pressure falls below the tensile strength of the liquid, transient cavitation nuclei form within the liquid, leading to bubble nucleation and subsequent expansion during the same stage. In the compression half-cycle, these cavitation nuclei rapidly contract and eventually collapse (Parvizian et al., 2011; Adewuyi and Khan, 2012), generating shock jets and shock waves (Monnier et al., 1999). This phenomenon is referred to as the cavitation effect of ultrasonic waves (Fig. S4 of the ESM).

The ultrasonic cavitation effect plays a dual role in enhancing mineralization efficiency. The microjet causes multi-mode mechanical damage to the product composite layer (C-S-H/$CaCO_3$) on the surface of cement particles: when the shear stress exceeds the interfacial binding energy of the composite layer, the layered structure is peeled from the matrix; the stress concentration effect induces the initiation of microcracks at the brittle calcite grain boundaries, which propagate along the crystal cleavage planes; the crack network connects to form three-dimensional permeable channels, reconstructing the pore structure and enhancing the ion diffusion efficiency, resulting in microcracks and pore channels, thereby delaying the densification process of the product composite layer. This prolongs the plateau period, maintaining a high Ca^{2+} leaching rate (Fig. 10). Previous pH measurements indicate that the onset of passivation—where mineralization efficiency begins to decline—occurs at 9 min for the non-ultrasonic group, compared to 17 min for the ultrasonic-assisted group. Furthermore, although the temperature

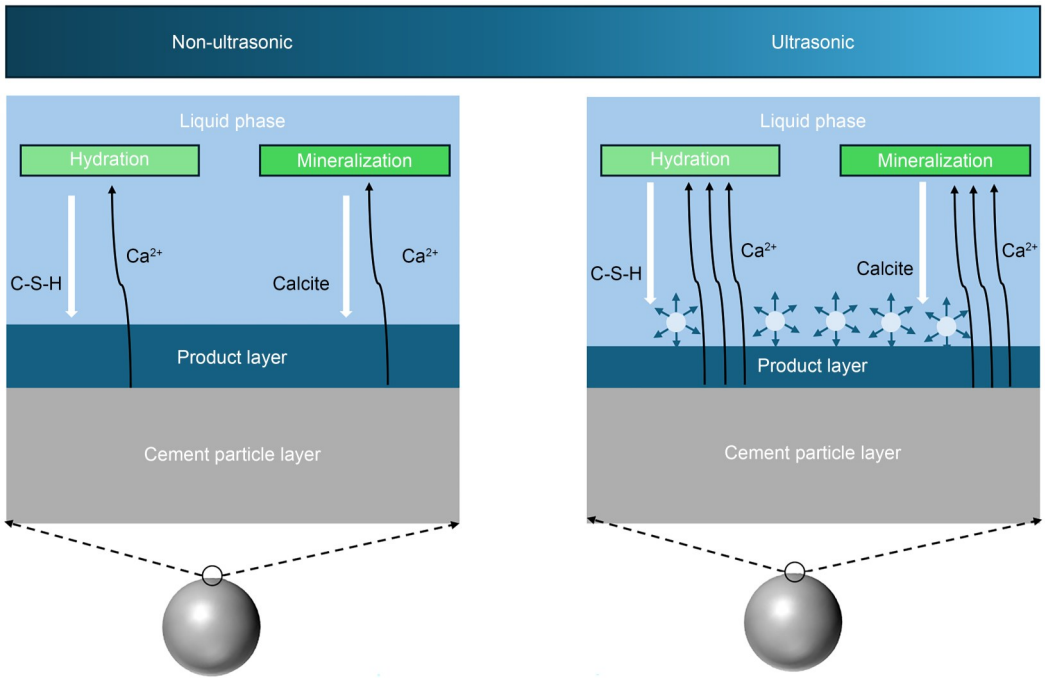

Fig. 10 Stripping of the composite layer by ultrasonic action

increase induced by the ultrasonic thermal effect reduces CO_2 solubility, it significantly enhances the ion diffusion rate within the suspension. Overall, this thermal effect exerts a positive influence on mineralization efficiency. This conclusion aligns with recent research findings (Mao et al., 2023), which indicate that under consistent CO_2 flow rate conditions at temperatures below 80 °C, moderate heating promotes the degree of wet mineralization. The enhanced diffusion resulting from temperature elevation effectively compensates for the potential negative impact caused by reduced solubility, thereby improving the efficiency of the mineralization reaction.

3.9.2 Strength enhancement mechanism of ultrasonic-assisted wet mineralization

The effects of ultrasonic accelerated hydration reaction and strength enhancement can be attributed to the following synergistic mechanisms. From the perspective of microscopic reaction, the shear stress induced by ultrasonic cavitation detaches some products from the product composite layer and imparts significant kinetic energy. These particles subsequently undergo intense collisions and friction, gradually reducing their size under ultrasonic refinement to reach the nanometer level (according to Fig. 10, the ultrasonic action on calcite crystals typically results in particle sizes less than 200 nm). Nanometer-sized particles exhibit higher specific surface areas and surface defect densities, which serve as active sites for the preferential adsorption of hydration reactants such as C_3S within the cement paste matrix. This reduces nucleation activation energy and accelerates the early hydration reaction process (Monkman et al., 2016). From a microscopic mechanics perspective, ultrasonic-assisted processes generate more C-S-H gels and calcite. These gels, combined with nanometer-sized calcite refined by ultrasonic treatment, exert a micro-aggregate effect, filling initial pores in the cement paste and providing strength support, thereby enhancing both the early and later strength of the cement paste.

Energy efficiency evaluation of ultrasonic action is presented in Section S2 of the ESM. Industrial application prospects and technical challenges is presented in Section S3 of the ESM. The specific process flow chart is shown in Fig. S5 of the ESM, and the specific energy efficiency calculation table for ultrasonic action is shown in Table S2 of the ESM.

4 Conclusions

In this study, we investigate and compare the microscopic characteristics of ultrasonic-assisted and non-ultrasonic-assisted wet mineralized cement suspensions, as well as their effects on the compressive strength and setting time of cement paste after partially substituting the cement content. The following conclusions can be drawn:

1. The change in pH of a cement suspension during wet mineralization can be systematically categorized into three distinct stages: (1) a rapid drop, where CH generated from pre-mixing hydration reacts rapidly with CO_2, causing a sharp decline in pH from 11.7 to about 8.0; (2) a plateau, characterized by a stable pH range of 8.0–8.5 (ultrasonic-assisted wet mineralization has been shown to extend this stage by 89%); (3) a gradual decline, marked by a slow decrease in pH as CO_2 approaches saturation within the suspension.

2. Calcite is confirmed as the predominant mineral phase in the cement suspension after wet mineralization. Under identical wet mineralization durations, the calcite content is substantially increased by applying the ultrasonic-assisted method. During the process of wet mineralization, a synergistic reaction between mineralization and hydration occurs. We find that within the same mineralization time, UC-2-25 has a 16.02% higher C-S-H content than MC-2-25.

3. Following the substitution of a portion of the cement pastes with the wet mineralized cement suspension, the cement paste demonstrates an increase in compressive strength and exhibits enhanced early-strength properties. The maximum 1-d strength of the cement paste is increased by 25.78%, the initial setting time is shortened by 19.46%, and the final setting time is shortened by 12.98%. Within the same mineralization time, the 28-d compressive strength of UC-2-25 is 3.95 PPs higher than that of MC-2-25. UC-2-15 exhibits the maximum improvement in compressive strength. Compressive strength does not increase linearly with prolonged mineralization time, but shows a specific gain threshold. UC-2-15 exhibits the maximum improvement in compressive strength.

4. Ultrasonic action improves the mineralization efficiency of the suspension, and the wet mineralized suspension with ultrasonic assistance has stronger mineralization ability. UC-2-25 exhibits the highest degree of mineralization (53.12%), surpassing

MC-2-25 (non-ultrasonic-assisted wet mineralization) by 13.78 PPs under the same mineralization time. This may be attributed to ultrasonic treatment inhibiting large crystal growth and inducing a thermal effect that accelerates the reaction rate.

Acknowledgment

This work is supported by the Pioneer R&D Program of Zhejiang Province, China (No. 2022C03040) and the Key Research and Development Program of Hangzhou, China (No. 202204T15).

Author contributions

Yongsheng CHEN drafted the paper and conducted the investigation, validation, formal analysis, and data curation. Fengping YU conducted the investigation, methodology, and visualization. Yanbiao ZHU conducted the methodology. Hedong LI reviewed and edited the paper, supervised the study, administered the project, developed the methodology, acquired the funding, and conceptualized the research. Tao WANG conceptualized the research and acquired the funding.

Conflict of interest

Yongsheng CHEN, Fengping YU, Yanbiao ZHU, Hedong LI, and Tao WANG declare that they have no conflict of interest.

Reference

Adewuyi YG, Khan NE, 2012. Modeling the ultrasonic cavitation-enhanced removal of nitrogen oxide in a bubble column reactor. *AIChE Journal*, 58(8):2397-2411. https://doi.org/10.1002/aic.12751

Aghajanian S, Nieminen H, Laari A, et al., 2021. Integration of a calcium carbonate crystallization process and membrane contactor–based CO_2 capture. *Separation and Purification Technology*, 274:119043. https://doi.org/10.1016/j.seppur.2021.119043

Andrade C, Sanjuán MÁ, 2021. Carbon dioxide uptake by pure Portland and blended cement pastes. *Developments in the Built Environment*, 8:100063. https://doi.org/10.1016/j.dibe.2021.100063

Ashraf W, 2016. Carbonation of cement-based materials: challenges and opportunities. *Construction and Building Materials*, 120:558-570. https://doi.org/10.1016/j.conbuildmat.2016.05.080

Chang J, Wang D, Fang YF, 2018. Effects of mineralogical changes in BOFS during carbonation on pH and Ca and Si leaching. *Construction and Building Materials*, 192:584-592. https://doi.org/10.1016/j.conbuildmat.2018.10.057

Dong ZY, Yao CQ, Zhang YC, et al., 2016. Hydrodynamics and mass transfer of oscillating gas-liquid flow in ultrasonic microreactors. *AIChE Journal*, 62(4):1294-1307. https://doi.org/10.1002/aic.15091

Fagerlund J, Highfield J, Zevenhoven R, 2012. Kinetics studies on wet and dry gas–solid carbonation of MgO and $Mg(OH)_2$ for CO_2 sequestration. *RSC Advances*, 2(27):10380-10393. https://doi.org/10.1039/C2RA21428H

Fernández-Carrasco L, Torrens-Martín D, Morales LM, et al., 2012. Infrared spectroscopy in the analysis of building and construction materials. *In*: Theophanides T (Ed.), Infrared Spectroscopy - Materials Science, Engineering and Technology. InTech, Rijeka, Croatia. https://doi.org/10.5772/36186

Fu XX, Guerini A, Zampini D, et al., 2024. Storing CO_2 while strengthening concrete by carbonating its cement in suspension. *Communications Materials*, 5(1):109. https://doi.org/10.1038/s43246-024-00546-9

Gartner E, Hirao H, 2015. A review of alternative approaches to the reduction of CO_2 emissions associated with the manufacture of the binder phase in concrete. *Cement and Concrete Research*, 78:126-142. https://doi.org/10.1016/j.cemconres.2015.04.012

Goergens J, Manninger T, Goetz-Neunhoeffer F, 2020. In-situ XRD study of the temperature-dependent early hydration of calcium aluminate cement in a mix with calcite. *Cement and Concrete Research*, 136:106160. https://doi.org/10.1016/j.cemconres.2020.106160

Günther C, Becker A, Wolf G, et al., 2005. In vitro synthesis and structural characterization of amorphous calcium carbonate. *Zeitschrift für Anorganische und Allgemeine Chemie*, 631(13-14):2830-2835. https://doi.org/10.1002/zaac.200500164

Hamidi H, Mohammadian E, Haddad AS, et al., 2017. Effects of ultrasonic waves on carbon dioxide solubility in brine at different pressures and temperatures. *Petroleum Science*, 14(3):597-604. https://doi.org/10.1007/s12182-017-0165-2

He Z, Li Z, Shao YX, 2017. Effect of carbonation mixing on CO_2 uptake and strength gain in concrete. *Journal of Materials in Civil Engineering*, 29(10):04017176. https://doi.org/10.1061/(ASCE)MT.1943-5533.0002031

Li L, Wu M, 2022. An overview of utilizing CO_2 for accelerated carbonation treatment in the concrete industry. *Journal of CO_2 Utilization*, 60:102000. https://doi.org/10.1016/j.jcou.2022.102000

Li WZ, Cao ML, Wang D, et al., 2023. Improving the hydration activity and volume stability of the RO phases in steel slag by combining alkali and wet carbonation treatments. *Cement and Concrete Research*, 172:107236. https://doi.org/10.1016/j.cemconres.2023.107236

Lippiatt N, Ling TC, Pan SY, 2020. Towards carbon-neutral construction materials: carbonation of cement-based materials and the future perspective. *Journal of Building Engineering*, 28:101062. https://doi.org/10.1016/j.jobe.2019.101062

Liu LL, Ji YS, Ma ZG, et al., 2021. Study on the effects of ultrasonic agitation on CO_2 adsorption efficiency improvement of cement paste. *Applied Sciences*, 11(15):6877. https://doi.org/10.3390/app11156877

Liu SH, Zhang HB, Wang YL, et al., 2021a. Carbon-dioxide-activated bonding material with low water demand. *Advances in Cement Research*, 33(5):193-196.

https://doi.org/10.1680/jadcr.18.00222

Liu SH, Shen PL, Xuan DX, et al., 2021b. A comparison of liquid-solid and gas-solid accelerated carbonation for enhancement of recycled concrete aggregate. *Cement and Concrete Composites*, 118:103988. https://doi.org/10.1016/j.cemconcomp.2021.103988

Mao YG, He PP, Drissi S, et al., 2023. Effect of conditions on wet carbonation products of recycled cement paste powder. *Cement and Concrete Composites*, 144:105307. https://doi.org/10.1016/j.cemconcomp.2023.105307

Mehdipour I, Falzone G, La Plante EC, et al., 2019. How microstructure and pore moisture affect strength gain in portlandite-enriched composites that mineralize CO_2. *ACS Sustainable Chemistry & Engineering*, 7(15):13053-13061. https://doi.org/10.1021/acssuschemeng.9b02163

Monkman S, MacDonald M, Hooton RD, et al., 2016. Properties and durability of concrete produced using CO_2 as an accelerating admixture. *Cement and Concrete Composites*, 74:218-224. https://doi.org/10.1016/j.cemconcomp.2016.10.007

Monnier H, Wilhelm AM, Delmas H, 1999. The influence of ultrasound on micromixing in a semi-batch reactor. *Chemical Engineering Science*, 54(13-14):2953-2961. https://doi.org/10.1016/S0009-2509(98)00335-2

Parvizian F, Rahimi M, Faryadi M, 2011. Macro- and micromixing in a novel sonochemical reactor using high frequency ultrasound. *Chemical Engineering and Processing: Process Intensification*, 50(8):732-740. https://doi.org/10.1016/j.cep.2011.06.011

Sáez Del Bosque IF, Martínez-Ramírez S, Blanco-Varela MT, 2014. FTIR study of the effect of temperature and nanosilica on the nano structure of C-S-H gel formed by hydrating tricalcium silicate. *Construction and Building Materials*, 52:314-323. https://doi.org/10.1016/j.conbuildmat.2013.10.056

Shen PL, Zhang YY, Jiang Y, et al., 2022a. Phase assemblance evolution during wet carbonation of recycled concrete fines. *Cement and Concrete Research*, 154:106733. https://doi.org/10.1016/j.cemconres.2022.106733

Shen PL, Lu JX, Zhang YY, et al., 2022b. Preparation aragonite whisker-rich materials by wet carbonation of cement: towards yielding micro-fiber reinforced cement and sequestrating CO_2. *Cement and Concrete Research*, 159:106891. https://doi.org/10.1016/j.cemconres.2022.106891

Steinour HH, 1959. Some effects of carbon dioxide on mortars and concrete-discussion. *Journal of American Concrete Institute*, 30(2):905-907.

Sulistiyono E, Handayani M, Arwanda MR, et al., 2019. Fabrication of nano-calcium carbonate precipitate by ultrasonic milling technique using ethylene glycol media. *IOP Conference Series: Materials Science and Engineering*, 578(1):012038. https://doi.org/10.1088/1757-899X/578/1/012038

Tamidi AM, Lau KK, Khalit SH, 2021. A review of recent development in numerical simulation of ultrasonic-assisted gas-liquid mass transfer process. *Computers & Chemical Engineering*, 155:107498. https://doi.org/10.1016/j.compchemeng.2021.107498

Wang D, Chang J, 2019. Comparison on accelerated carbonation of β-C_2S, $Ca(OH)_2$, and C_4AF: reaction degree, multi-properties, and products. *Construction and Building Materials*, 224:336-347. https://doi.org/10.1016/j.conbuildmat.2019.07.056

Wang ML, Luo S, Pham BT, et al., 2023. Effect of CO_2-mixing dose and prolonged mixing time on fresh and hardened properties of cement pastes. *Journal of Zhejiang University-SCIENCE A*, 24(10):886-897. https://doi.org/10.1631/jzus.A2200571

Xiong GQ, Wang C, Zhou S, et al., 2023. Understanding the thermal effect of power ultrasound in cement paste. *Applied Thermal Engineering*, 232:120946. https://doi.org/10.1016/j.applthermaleng.2023.120946

Xiong GQ, Ren YL, Jia XL, et al., 2024. Understanding the influence of ultrasonic power on the hydration of cement paste. *Journal of Building Engineering*, 87:108996. https://doi.org/10.1016/j.jobe.2024.108996

Xu ZS, Ji YS, Ma ZG, et al., 2023. Strengthening mechanism of ultrasonic action on mechanical properties of cement-based materials. *Construction and Building Materials*, 362:129788. https://doi.org/10.1016/j.conbuildmat.2022.129788

Zajac M, Skibsted J, Skocek J, et al., 2020. Phase assemblage and microstructure of cement paste subjected to enforced, wet carbonation. *Cement and Concrete Research*, 130:105990. https://doi.org/10.1016/j.cemconres.2020.105990

Zou ZY, Bertinetti L, Politi Y, et al., 2015. Opposite particle size effect on amorphous calcium carbonate crystallization in water and during heating in air. *Chemistry of Materials*, 27(12):4237-4246. https://doi.org/10.1021/acs.chemmater.5b00145

Electronic supplementary materials

Sections S1–S3, Figs. S1–S5, Tables S1 and S2